



Electronic states and intraband terahertz optical transitions in InGaAs quantum rods

Nikola Prodanović, Nenad Vukmirović, Dragan Indjin, Zoran Ikonić, and Paul Harrison

Citation: *J. Appl. Phys.* **111**, 073110 (2012); doi: 10.1063/1.3692069

View online: <http://dx.doi.org/10.1063/1.3692069>

View Table of Contents: <http://jap.aip.org/resource/1/JAPIAU/v111/i7>

Published by the [American Institute of Physics](http://www.aip.org).

Related Articles

Optically controlled spin-dependent Andreev reflection and spin accumulation in a quantum dot

J. Appl. Phys. **111**, 083706 (2012)

The electronic properties of a core/shell/well/shell spherical quantum dot with and without a hydrogenic impurity

J. Appl. Phys. **111**, 083702 (2012)

Thermal emission in type-II GaSb/GaAs quantum dots and prospects for intermediate band solar energy conversion

J. Appl. Phys. **111**, 074514 (2012)

Conditional photon-assisted transport in coupled quantum dot

Appl. Phys. Lett. **100**, 153105 (2012)

Tuning of mid-infrared emission of ternary PbSrTe/CdTe quantum dots

Appl. Phys. Lett. **100**, 113112 (2012)

Additional information on *J. Appl. Phys.*

Journal Homepage: <http://jap.aip.org/>

Journal Information: http://jap.aip.org/about/about_the_journal

Top downloads: http://jap.aip.org/features/most_downloaded

Information for Authors: <http://jap.aip.org/authors>

ADVERTISEMENT

**FIND THE NEEDLE IN THE
HIRING HAYSTACK**

Post jobs and reach
thousands of hard-to-find
scientists with specific skills



<http://careers.physicstoday.org/post.cfm> **physicstoday JOBS**

Electronic states and intraband terahertz optical transitions in InGaAs quantum rods

Nikola Prodanović,^{1,a)} Nenad Vukmirović,² Dragan Indjin,¹ Zoran Ikonić,¹
and Paul Harrison¹

¹*Institute of Microwaves and Photonics, School of Electronic and Electrical Engineering, University of Leeds, Woodhouse Lane, Leeds LS2 9JT, United Kingdom*

²*Scientific Computing Laboratory, Institute of Physics Belgrade, University of Belgrade, Pregrevica 118, 11080 Belgrade, Serbia*

(Received 30 August 2011; accepted 9 February 2012; published online 11 April 2012)

Strain-dependent eight-band $k \cdot p$ method is used to analyze the electronic structure and intraband optical transitions in self-assembled InGaAs quantum rods in the terahertz range. The calculation of absorption spectra for the growth- and in-plane-polarized radiation shows some similarities to those of quantum well and single quantum dot structures, augmented with contribution from transitions between the dot and quantum well states. The influence of rod height on the electronic structure and the intraband absorption spectra is also investigated. It is found that the energy of maximal terahertz absorption can be tailored by the rod height for both in-plane and in-growth polarized radiation. © 2012 American Institute of Physics. [<http://dx.doi.org/10.1063/1.3692069>]

I. INTRODUCTION

Semiconductor quantum dots are continuously attracting significant research interest, because their properties can be engineered, via their structural parameters, allowing the design of dots with electronic and optical properties suited to a particular application. In many cases, they are expected to offer better performance than similar devices based on quantum wells and wires. The growth of such structures is typically in the Stranski-Krastanov mode, which produces self-assembled dots with the height-to-diameter aspect ratio well below one and without a precise controllability of their size.

Novel quantum nanostructures—quantum rods or quantum posts—have recently been realized.^{1–4} In contrast to self-assembled quantum dots with typical heights of a few nanometers, quantum rods can be grown with heights up to several tens of nanometers. They have quite large aspect ratios, the controllability of which is achieved by alternating deposition of very short (of the order of monolayer) layers of InAs and GaAs. Subsequent intermixing of InAs and GaAs leads to InGaAs quantum rods with large and precisely tunable aspect ratio. Recent experiments on carrier capture dynamics in quantum rod structures⁵ suggest that quantum rods may be very promising for future device applications. There is also a very recent report⁶ that charged quantum rods embedded in a quantum well matrix give rise to a “perforated” electron gas. Additional growth control by using different arsenic sources has been reported.^{7,8}

It is, therefore, of interest to develop a full theoretical description of electronic and optical properties, which would enable the purpose engineering of quantum rod-based structures. Initial work in this area has focused on calculation of energy levels and interband optical properties,^{1,2,9} as well as theoretical investigation of dominant physical effects affect-

ing their interband optical properties.¹⁰ We have recently performed preliminary work on calculation of intraband (intersubband) absorption in the THz spectral range.¹¹ Following the recent experimental observation and theoretical analysis of terahertz ionization of highly charged quantum posts,⁶ in this work, we focus on detailed simulations of THz intraband optical absorption of polarized radiation at extremely low and liquid nitrogen temperatures. Within this scope, it suffices to consider the rod electronic structure alone, neglecting the formation of polaron states discussed in Ref. 12, because the spectrum of polaron states is not significantly different from a pure electronic spectrum in terms of optical probing.

We first briefly describe the strain-dependent eight-band $k \cdot p$ model for the electronic structure and the absorption cross sections calculation. The results are also compared to those obtained within the simple effective mass model, the latter being quite useful for qualitative insight.

II. THEORETICAL MODEL

A. Electronic structure: Eight band $k \cdot p$ model

The electronic structure of quantum rods is calculated within the eight-band envelope function $k \cdot p$ model.^{13–17} The strain distribution was found within the continuum mechanical model,¹⁸ with the calculation based on the finite element method.¹⁹

As for the rod cross section, both the cylindrical^{5,6,20} and square-based¹ shapes were reported. Yet, in our previous study of InGaAs quantum dots,²¹ we have shown that the intraband absorption spectrum is essentially the same for truncated square-based pyramids and truncated cones. This indicates that the details of the base shape (square versus circle) are not very important and have assumed the cylindrically shaped rods in our simulations, which should capture the essential features of an intraband absorption spectra of rods with different cross sections. Such an approximation is

^{a)}Electronic mail: elnpr@leeds.ac.uk.

further supported by the fact that, as described in Sec. II B–Sec. IV, the main features of bound-to-bound optical transitions are the same in the simple effective mass particle-in-a-box model for a square-based rod and in the full simulation with a cylindrical rod, and it is even less likely that the properties of unbound states are significantly affected by the exact shape of the rod base.

With the cylindrical shape of rods assumed, the axial approximation²¹ was used. The Hamiltonian eigenvalue problem was then solved using the orthonormal function expansion, where the basis was formed from the direct product of Bessel functions in the radial direction and plane waves in the growth (z) direction. The cylindrical symmetry of the rods introduces a good quantum number (m_f), describing the z – component of the total quasi-angular momentum, which takes half-integer values.^{21,22} The optical transition selection rules then allow only the transitions with $\Delta m_f = 0$ in the case of z – polarised radiation and $|\Delta m_f| = 1$ for the in-plane, e.g., x – polarised radiation.

The calculated electronic structure is then used to find the intraband absorption spectra. The case of $T = 0$ has been investigated previously,¹¹ assuming that only the ground state is occupied (the two-fold degeneracy of $|m_f|$ states then implies that no more than two electrons can be present in the quantum rod). In this work, we consider the lattice temperatures of either 0 K or 77 K. The latter case allows thermal population of higher states and absorption from these states as well. The inhomogeneity of the quantum rod ensemble (fluctuations of rod size and deviations of the base shape from perfect circular or square) gives contribution to transition linewidths and is taken into account by assuming a Gaussian line shape with a standard deviation σ equal to 10% of the transition energy, i.e., $\sigma = 0.1(E_f - E_i)$.

Under equilibrium conditions, a transition in the quantum rod has the effective absorption cross-section,

$$\sigma_e(i \rightarrow f) = \frac{2\pi\hbar}{\tilde{n}\epsilon_0 c E} \left| \frac{\langle i | \hat{H}' | f \rangle}{A} \right|^2 \frac{1}{\sigma\sqrt{2\pi}} \times \exp\left(-\frac{(E - (E_f - E_i))^2}{2\sigma^2}\right) \Theta_{if}, \quad (1)$$

where i and f denote the initial and final state and \tilde{n} the refractive index. The dipole perturbation $\hat{H}' = \frac{e}{m_0} \hat{\mathbf{p}} \cdot A\epsilon$ depends on the incident radiation magnetic vector potential A and its polarization unit vector ϵ , and Θ_{if} is the difference of the initial and final state population,

$$\Theta_{if} = \frac{1}{\exp\frac{(E_i - E_F)}{k_b T} + 1} - \frac{1}{\exp\frac{(E_f - E_F)}{k_b T} + 1},$$

where E_F is the Fermi level, determined by the average number of electrons in a rod.

B. Effective mass model

For a simple picture of phenomena observed in the detailed calculation, we also give a simple effective-mass

model of the electronic structure, dipole matrix elements, and optical cross-sections for states confined in the dot or in the well embedding the dot.

Consider a cuboidal quantum dot embedded in an infinite potential barrier with a square base of side length a and height d . Envelope functions of its eigenstates are

$$\Psi_i(x, y, z) = \frac{2\sqrt{2}}{a\sqrt{d}} \sin\left(\frac{xn_x^i\pi}{a}\right) \sin\left(\frac{yn_y^i\pi}{a}\right) \sin\left(\frac{zn_z^i\pi}{d}\right) \quad (2)$$

and the corresponding energies,

$$E_i = \frac{\pi^2\hbar^2}{2m^*a^2} ((n_x^i)^2 + (n_y^i)^2) + \frac{\pi^2\hbar^2}{2m^*d^2} (n_z^i)^2. \quad (3)$$

Similarly, in an infinitely deep quantum well, the eigenstates are

$$\Psi_{k_x, k_y, n}(x, y, z) = \frac{\sqrt{2}}{a\sqrt{d}} e^{ik_x x} e^{ik_y y} \sin\left(\frac{zn\pi}{d}\right) \quad (4)$$

and the corresponding energies

$$E_{k_x, k_y, n} = \frac{\hbar^2}{2m^*} (k_x^2 + k_y^2) + \frac{\pi^2\hbar^2}{2m^*d^2} n^2, \quad (5)$$

where (k_x, k_y) is the in-plane wave vector and the quantum number n counts the subbands.

In order to use Eq. (1), one requires the momentum matrix element $\mathbf{p}_{if} = \int \Psi_i \hat{\mathbf{p}} \Psi_f d\mathbf{r}$. For light polarization, $\epsilon = \epsilon_x \mathbf{i} + \epsilon_z \mathbf{k}$, where z is the growth and x the in-plane direction, the momentum matrix elements are straightforwardly found as

$$p_{if}^x = \begin{cases} 4i\hbar \frac{\phi_{if}^x}{a} & \text{for } (n_x^i - n_x^f) \text{ odd} \\ 0 & \text{for } (n_x^i - n_x^f) \text{ even} \end{cases}, \quad (6a)$$

$$p_{if}^z = \begin{cases} 4i\hbar \frac{\phi_{if}^z}{d} & \text{for } (n_z^i - n_z^f) \text{ odd} \\ 0 & \text{for } (n_z^i - n_z^f) \text{ even} \end{cases}, \quad (6b)$$

where

$$\phi_{if}^x = \epsilon_x \delta_{n_x^i n_x^f} \delta_{n_z^i n_z^f} \frac{n_x^i n_x^f}{(n_x^i)^2 - (n_x^f)^2},$$

$$\phi_{if}^z = \epsilon_z \delta_{n_x^i n_x^f} \delta_{n_y^i n_y^f} \frac{n_z^i n_z^f}{(n_z^i)^2 - (n_z^f)^2}.$$

All selection rules are included in Eqs. (6a) and (6b).

For the quantum well surrounding the dot, the only non-zero matrix element is

$$P_{k_x, k_y, n, k_x', k_y', m}^z = \begin{cases} 4i\epsilon_z \frac{\hbar}{d} \delta_{k_x k_x'} \delta_{k_y k_y'} \frac{mn}{m^2 - n^2} & \text{for } (m - n) \text{ odd} \\ 0 & \text{for } (m - n) \text{ even} \end{cases}. \quad (7)$$

III. NUMERICAL RESULTS AND DISCUSSION

A. Electronic structure

The electronic structure of quantum rods was calculated using the 8-band $k \cdot p$ envelope function model. The rod material composition and geometric parameters were taken in accordance with the literature data. The rod diameter was taken to be 10 nm,¹ and the rod height was varied from 2.5 nm to 60 nm, which covers the typical range of quantum rod heights.^{1,2} The InAs/GaAs short-period superlattice, away from the quantum rod, transforms into an InGaAs alloy quantum well layer with In content of 16%¹ during the structure growth. The In content in the rod is approximately 45%.¹ The profile of the cylindrically symmetric structure in the $z-r$ plane is schematically shown in the inset of Fig. 1, and the conduction band edge profile in the growth direction for $r = 0$ (which includes the hydrostatic strain-induced shift) is shown in Fig. 1. The structure can be considered as a quantum well with the z axis as the growth direction and with the potential getting deeper in the radial direction, up to the rod radius of $r = 5$ nm.

The electronic structure of 60-nm- and 10-nm-high rods is displayed in Fig. 2, together with the wavefunction moduli squared for a number of relevant states. The electronic states can be classified as either free or non-free, according to whether their energies are above or below the barrier in the growth direction.

Numerical calculations were performed in the subspace defined by basis functions corresponding to the closed box around the whole structure, and these solutions make a discrete set. For quasi-bound and free states, this description is clearly only approximate, but one can still expect that such discretisation, in fact, samples the continuum (including the resonances) of the open system and should be able to capture the variation of optical transition matrix elements with the transition energy. All non-free states can be further divided into three subgroups. The first subgroup, labeled with A in Fig. 2, includes states completely localized in the dot, which exist only due to the dot. Their total energies do not have to be lower than the barrier in the radial direction, as is the case, e.g., for state A_4 for the 60-nm-high rod or state A_2 for

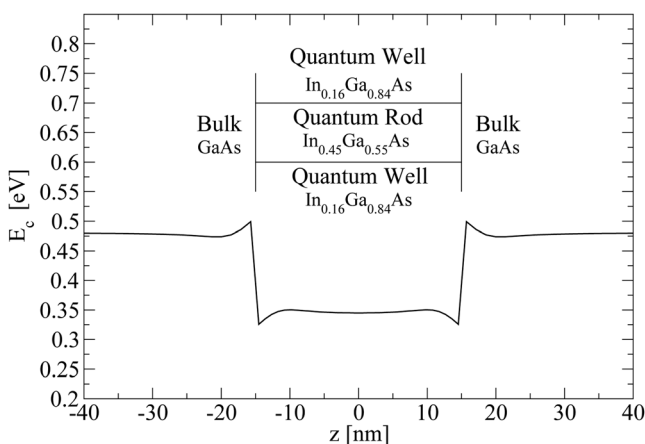


FIG. 1. The conduction band profile, including the hydrostatic strain potential, for a 30-nm-tall quantum rod. The structure layout in the $z-r$ plane is shown in the inset.

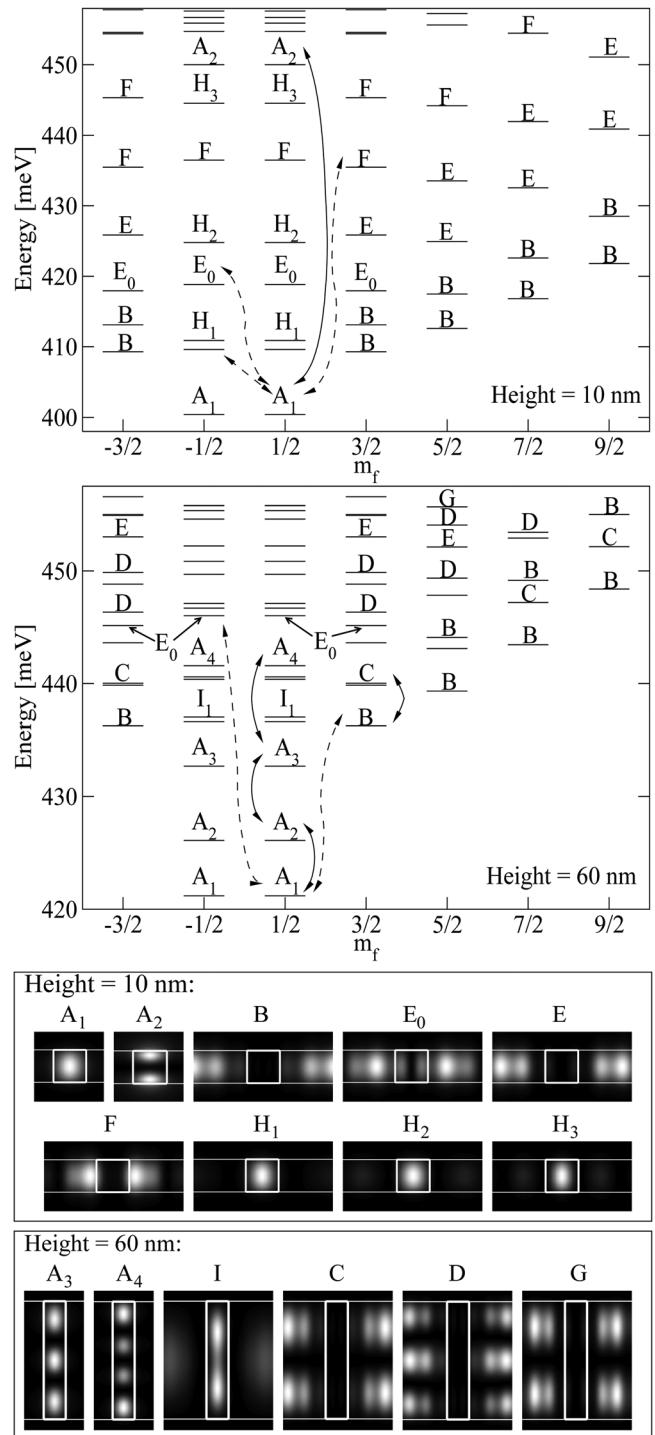


FIG. 2. Energy diagrams for quantum rods with 10 nm height (upper) and 60 nm height (the lower diagram). Different types of states have different (but height-independent) labels. The lower part of the figure shows various types of states (wavefunction structures) appearing in the quantum rods. Solid (dashed) double-headed lines indicate the dominant transitions for the z -(in-plane) polarized radiation.

the 10-nm-high rod (a part of their energy comes from quantisation in the z -direction). Since the In content-related barrier in the radial direction is about 30% lower than in the growth direction, these states behave like bound states in an infinite dot, described by Eq. (2). Increasing n_z increases the number of nodes in the growth direction. The quantum number m_f plays a role similar to quantum numbers n_x and n_y .

According to Eqs. (6a), (6b), and (7), only the transitions between the bound dot states, i.e., from (the only significantly populated) $m_f = \frac{1}{2}$ and $m_f = -\frac{1}{2}$ into higher states (observing the selection rules), can significantly contribute to absorption of radially polarized radiation. Dot states with higher values of m_f are absent.

Within the simple effective-mass model, those states would be described by the quantum numbers $n_x = 1$ and $n_y = 1$. For taller rods, the energy difference between these bound states decreases (Eq. (3)). This can be also seen from Fig. 2, where states A_1 , A_2 , and A_3 in 60-nm-high rods have energies lower than the radial barrier, but in the 10-nm-high rod, the p -like bound state A_2 is far above the s -like A_1 , with energy higher than the radial barrier. This is a very interesting feature. State A_2 is bound, although its energy is in the subband continuum. This indicates that an electron optically excited into A_2 state might be efficiently extracted by a lateral electric field, which will be discussed later on. The third state, A_3 , does not exist in the 10-nm-high rod, since the number of bound states in the well and the dot is reduced by decreasing the height of the dot, i.e., by decreasing the well width.

The second subgroup of non-free states appears for energies higher than the radial barrier, and these states are completely localized outside the rod. Their properties are determined by the well and will be hereafter called well states. These states are, actually, quantum well bound states behaving like plane waves in the radial direction and can be classified into subbands according to Eq. (4) and Eq. (5). Among the well states, one can recognize states from the same subband, because they look similarly, i.e., have the same number of nodes in the growth direction and similar wave-like behavior in the radial direction. Therefore, B, C, and D in Fig. 2 denote the 1st, 2nd, and 3rd subband in the growth direction. All these states behave like plane waves in the radial direction. Figure 2 shows that increasing the quantum number m_f gives states lined up along a parabolic “subband”. This is fully analogous to the wave in the radial (x or y) direction and its parabolic dispersion with k_x and k_y in a simple infinitely deep well.

The same as for the dot states, the energy difference between quantum well states within different subbands, but with the same m_f , decreases as the rod height increases (Eq. (5)). There are also a larger number of subbands in the well, causing complicated state ordering for taller rods. The density of states increases, leading to interlacing of states from different subbands (Fig. 2).

The third subgroup of non-free states, denoted as mixed states, are those which are only partially localized in the dot. For example, one of those states is labeled as the E_0 -state in Fig. 2. These largely delocalised states are denoted as E, F, and G and also form bands in the same way as B, C, and D states do, but their behavior in the radial direction is different. States E, F, and G are not homogeneous waves in the radial direction, although they are not localized either. Furthermore, their energy depends only mildly on the quantum rod and quantum well parameters. The state E_0 behaves as the ground state for the quasi-subband E. We also note that states F_0 and G_0 , as ground states for subbands F and G, could be added on the diagram, but they are not labeled in Fig. 2, since their exact nature is less clear.

There also exist non-free states labeled as H for the 10-nm-high rod and as I for the 60-nm-high rod in Fig. 2. Those states are partially localized outside the rod, but their shape is still largely influenced by the rod. Some of those states have no nodes in the growth direction, like H states, or one node, like I states, which indicates the order of their quantization. It is difficult to find a precise qualitative description or unambiguous classification of these states.

To conclude, by varying the height of the quantum rod structure, one can tune the energy spacing between various bound states. The spacing between consecutive dot bound states decreases with increasing the rod height. The same applies to the spacing between consecutive well states with the same m_f , but from different subbands. All that affects the ordering of states and enables tunability of absorption spectra for light polarized in the growth direction.

B. Intraband absorption spectra

All intra-subband transitions for in-plane, i.e., radially polarized radiation are forbidden (see Eq. (7)). From Eqs. (6a), (6b), and (7), it is clear that the momentum matrix elements depend only on the size of the structure in the direction of the light polarization, which, within the range of structures considered here, means that the absorption of z -polarized radiation will vary.

The lowest bound dot state is the ground state of the system and, except in the case of very long rods (e.g., 60 nm), the next couple of states belong to the first well subband, which can accommodate a number of electrons, due to their continuous nature. Assuming that the number of electrons per rod is small enough that only the ground dot state and the lowest subband states are significantly populated, the Fermi level is very close to the first subband minimum and the transitions from these states will give the major contribution to the total absorption.

What matters for a good photodetector performance are the transitions from the populated initial states to low-lying free states (resonances), because electrons in the latter can efficiently contribute to the current if the structure is biased. Yet, the cross-sections of these transitions may be very small compared to those for bound-to-bound transitions, according to Eq. (1), and this issue has to be investigated separately.

1. Absorption of z -polarized radiation

The absorption is strong only for transitions between opposite parity states, as is clear from the simple effective mass model (Eqs. (6b) and (7)). For example, according to Eq. (6b), one expects that the dominant matrix element for z -polarized radiation will be between the ground state with $n_x^i = 1$, $n_y^i = 1$, and $n_z^i = 1$ (s -like state) and $n_x^f = 1$, $n_y^f = 1$, and $n_z^f = 2$ (the p -like, also dot state, with a good overlap with the initial state), as the calculation indeed gives. The same rule applies to transitions between the well subbands, i.e., the matrix element is large for the transition between $n = 1$ and $n = 2$ states (Eq. (7)). As shown in Fig. 2 (solid double-arrowed lines), the dominant dipole matrix elements are usually between states of type A with opposite parity, e.g., $A_1 - A_2$, and between subbands B and C or C and D.

Increasing the dot height decreases both the momentum matrix element squared and the state spacing, and the latter dependence is stronger than the former, because it acts both explicitly and via the energy-dependent linewidth, resulting in increasing cross-section. This is predicted by both the full $\mathbf{k} \cdot \mathbf{p}$ and the simple effective mass model.

At higher temperatures, transitions from higher states of the quantum dot can also significantly contribute the total absorption, as they become increasingly populated. However, the absorption peak positions hardly change, because main additional transition, which was not active at $T = 0$ K, comes from the well states, and their spacing appears to be approximately the same as for the dot states.

Taller rods have a smaller state spacing, i.e., reduced transition energies of bound-to-bound transitions. Therefore, the absorption tunability for z -polarized radiation is achieved by changing the rod height for sufficiently tall rods, accommodating both an s -like and a p -like bound state.

This explains the cross-section for taller quantum rods calculated using Eq. (1), shown in Figs. 3 and 4. At $T = 0$ K, only the transitions from the dot ground, bound state, into the higher dot bound state exist (assuming a maximum of two electrons per dot). This is why a single peak appears for any height, shifting to lower frequency as height increases. At elevated temperatures, e.g., $T = 77$ K, an additional transition occurs from the first well subband, but at similar energies as transitions from the bound state. Therefore, Figs. 3 and 4 are generally similar. However, one can see from Fig. 4 that the absorption peak for the 60-nm-high rod decreases at elevated temperature, due to thermal population of the upper state. Clearly, taller rods with their small state spacings are more strongly affected by temperature.

The most interesting feature of intraband spectrum in this case is that, for a range of values of rod height, the dominant $s - p$ -like transition excites electrons into the quantum well continuum. These electrons can be efficiently extracted by a lateral electric field, thus providing a basis for the design of a lateral-extraction photodetector. The advantage of such a photodetector would be a strong bound-to-bound absorption

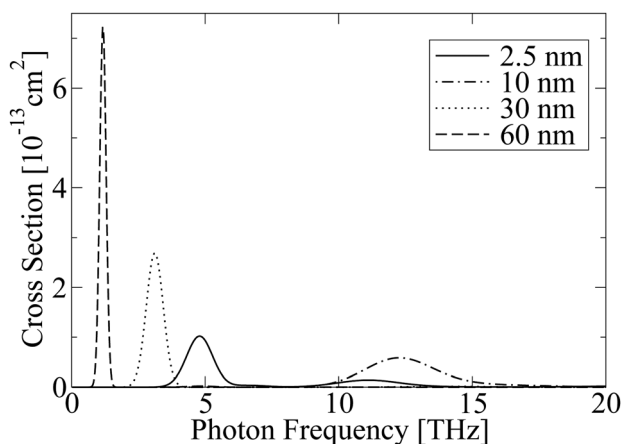


FIG. 3. Absorption cross-section for transitions from the ground state for z -polarized radiation at $T = 0$ K with one electron per rod. The absorption for the 2.5-nm-tall dot comes from the bound-to-continuum transition, since such a short dot can accommodate only one bound state. Absorption in taller rods comes from bound-to-bound transitions and follows the trend as the rod height varies.

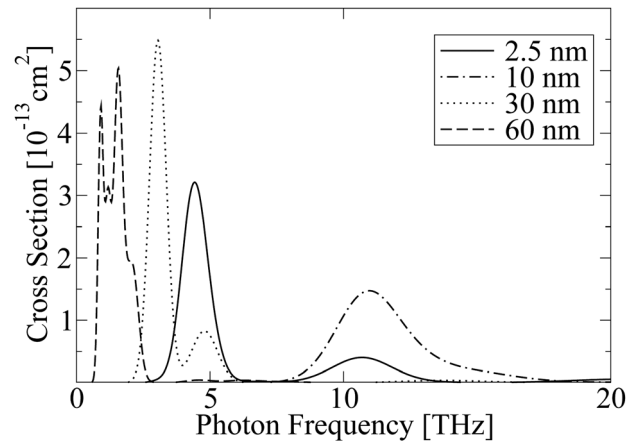


FIG. 4. Absorption cross-section for z -polarized radiation at $T = 77$ K with one electron per rod.

and an efficient continuum-like extraction of electrons. However, more detailed studies of electron transport are required before any more reliable conclusions can be made.

In the case of bound-to-continuum absorption, which can generate vertical photocurrent, the situation is quite different. Usually coming from transitions between non-subsequent states (in respect to size-quantization in the z -direction), this absorption may be quite small. The transition energy from the lowest bound to the barrier continuum state slowly decreases with increasing rod height. For larger matrix elements, one needs shorter rods, also evident from simple effective-mass model. For instance, the resonant bound-to-continuum absorption peak in the (rather flat) 2.5-nm-high quantum rod is comparable to bound-to-bound absorption. For higher rods (> 10 nm), however, bound-to-continuum absorption peaks are not observable on the same scale as bound-to-bound ones, due to the decreased values of momentum matrix elements, increased energy separation, and increased linewidth, which all lead to small absorption strength.

However, for extremely short rods, such as 2.5 nm (typical height of conventional quantum dots), the dominant transition for growth-polarized radiation is of bound-to-continuum type. These structures are not typical “rods”, and the results for them are given only for the sake of comparison between rods and conventional quantum dots.

2. Absorption of in-plane polarized radiation

The important issue in quantum well intraband photodetectors is that there is no absorption of in-plane polarized radiation, as is clear from Eq. (7). The quantum rod structure may have non-zero absorption of in-plane polarized radiation, e.g., based on transitions from the dot bound states with the quantum number $m_f = \frac{1}{2}$ into well and mixed states with $m_f = -\frac{1}{2}$.

The detailed examination of dominant optical matrix elements in the structure shows that transitions between bound states in the dot and higher well or mixed states, for the in-plane polarization, are more prominent than “intra-dot” transitions. With transitions between the subband states being forbidden, all absorption will come from transitions from the first bound state of the dot, with bound-to-bound transitions much stronger than bound-to-continuum transitions. The

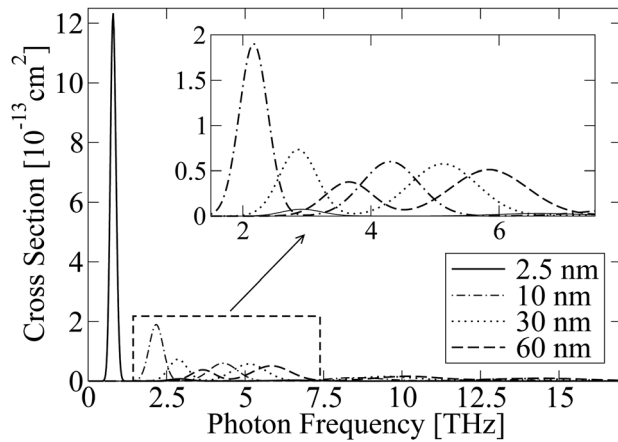


FIG. 5. Absorption cross-section for bound-to-bound transitions for in-plane polarized radiation at $T = 0$ K with one electron per rod.

bound-to-bound absorption peak can be tuned by changing the rod height, and results are shown in Fig. 5. Dominant transitions from the dot ground state are indicated with dashed double-headed lines in Fig. 2. Dominant bound-to-bound transitions in this case are transitions between A_1 and B or E_0 states.

The in-plane-polarized radiation can excite electrons into the well states. In contrast to the case of growth-polarization, the excited electrons are here already highly delocalized and easily extractable by lateral electric field. We conclude that a polarization-independent intraband lateral photodetector might be designed and optimized by a proper choice of rod height.

It is clear that the problem of small absorption strength for in-plane polarized radiation, compared to z -polarization, arises due to widely spread wavefunction of the mixed final state, which reduces the overlap with the initial dot bound state. The absorption peaks of bound-to-continuum transitions are also tunable with the rod height, same as in the case of z -polarization. Calculations show that the corresponding optical matrix elements increase with increasing dot height, in contrast to the case of z -polarization. For example, the first resonant bound-to-continuum transition in a 30-nm-high quantum rod has the transition matrix element similar to the bound-to-bound one at 3 THz, cf. Figure 5, and the situation remains like that down to the rod heights of ~ 10 nm, though not at 2.5 nm.

The opposite “direction” of the absorption peaks tunability for the two polarizations generally makes it possible to engineer the structure (find suitable rod height and diameter) so to get optimal functionality for both directions of incident radiation in the THz frequency range.

IV. CONCLUSION

In summary, a detailed strain-dependent eight-band $k \cdot p$ method was used to analyze the electronic structure and intraband optical properties of self-assembled quantum rods. It was found that their optical properties strongly depend on rod height, with an amount of tunability in terahertz frequency range, which enables engineering of these structures for optoelectronic applications. General features of the

absorption of z -polarized radiation are that it inherited properties of both an isolated quantum dot and a quantum well. The fact that p -like dot state is embedded in the well subband gives rise to the possibility of using the $s - p$ -like transitions in photodetection. The absorption of in-plane polarized radiation, which is due to electron transitions from the ground (dot-bound) state to the well states, is a benefit offered by this type of structures, in contrast to quantum wells. Such excited electrons can be efficiently extracted by lateral electric field, paving the way toward a polarization-independent lateral intraband terahertz photodetector.

ACKNOWLEDGMENTS

N.P. acknowledges the support in part by the University of Leeds Fully Funded International Research Scholarships program and in part by the Serbian Ministry of Education Scholarship program for students studying at the world’s leading universities. N.V. was supported in part by the Serbian Ministry of Science under project No. ON171017 and the European Commission under EU FP7 projects PRACE-IIP, HP-SEE, and EGI-InSPIRE. D.I., Z.I, and P.H. acknowledge support by NATO Science for Peace project EAP. SFFP 984068.

- ¹L. Li, G. Patriarche, N. Chauvin, P. Ridha, M. Rossetti, J. Andrzejewski, G. Sek, J. Misiewicz, and A. Fiore, *IEEE J. Sel. Top. Quantum Electron.* **14**, 1204 (2008).
- ²J. He, H. J. Krenner, C. Pryor, J. P. Zhang, Y. Wu, D. G. Allen, C. M. Morris, M. S. Sherwin, and P. M. Petroff, *Nano Lett.* **7**, 802 (2007).
- ³M. Motyka, G. Sek, K. Ryczko, J. Andrzejewski, J. Misiewicz, L. H. Li, A. Fiore, and G. Patriarche, *Appl. Phys. Lett.* **90**, 181933 (2007).
- ⁴P. Ridha, L. Li, A. Fiore, G. Patriarche, M. Mexis, and P. M. Smowton, *Appl. Phys. Lett.* **91**, 191123 (2007).
- ⁵D. Stehr, C. M. Morris, D. Talbayev, M. Wagner, H. C. Kim, A. J. Taylor, H. Schneider, P. M. Petroff, and M. S. Sherwin, *Appl. Phys. Lett.* **95**, 251105 (2009).
- ⁶C. M. Morris, D. Stehr, H. Kim, T.-A. Truong, C. Pryor, P. M. Petroff, and M. S. Sherwin, *Nano Lett.* **12**, 1115 (2012).
- ⁷L. H. Li, G. Patriarche, E. H. Linfield, S. P. Khanna, and A. G. Davies, *J. Appl. Phys.* **108**, 103522 (2010).
- ⁸R. Nedzinskas, B. Čechavičius, V. Karpus, J. Kavaliauskas, G. Valušis, L. H. Li, S. P. Khanna, and E. H. Linfield, *J. Appl. Phys.* **109**, 123526 (2011).
- ⁹T. Saito, H. Ebe, Y. Arakawa, T. Kakitsuka, and M. Sugawara, *Phys. Rev. B* **77**, 195318 (2008).
- ¹⁰J. Andrzejewski, G. Sęk, E. O’Reilly, A. Fiore, and J. Misiewicz, *J. Phys.: Conf. Ser.* **245**, 012038 (2010).
- ¹¹N. Prodanović, N. Vukmirović, D. Indjin, Z. Ikonić, and P. Harrison, *J. Phys.: Conf. Ser.* **242**, 012012 (2010).
- ¹²S. Hameau, J. N. Isaia, Y. Guldner, E. Deleporte, O. Verzellen, R. Ferreira, G. Bastard, J. Zeman, and J. M. Gérard, *Phys. Rev. B* **65**, 085316 (2002).
- ¹³T. B. Bahder, *Phys. Rev. B* **41**, 11992 (1990).
- ¹⁴S. Tomić, A. G. Sunderland, and I. J. Bush, *J. Mater. Chem.* **16**, 1963 (2006).
- ¹⁵N. Vukmirović, D. Indjin, V. D. Jovanović, Z. Ikonić, and P. Harrison, *Phys. Rev. B* **72**, 075356 (2005).
- ¹⁶V. Mlinar, M. Tadić, B. Partoens, and F. M. Peeters, *Phys. Rev. B* **71**, 205305 (2005).
- ¹⁷C. Pryor, *Phys. Rev. B* **57**, 7190 (1998).
- ¹⁸O. Stier, M. Grundmann, and D. Bimberg, *Phys. Rev. B* **59**, 5688 (1999).
- ¹⁹A. J. Davies, *The Finite Element Method* (Clarendon, Oxford, 1980).
- ²⁰H. Krenner, C. Pryor, J. He, J. Zhang, Y. Wu, C. Morris, M. Sherwin, and P. Petroff, *Physica E (Amsterdam)* **40**, 1785 (2008).
- ²¹N. Vukmirović, Ž. Gačević, Z. Ikonić, D. Indjin, P. Harrison, and V. Milanović, *Semicond. Sci. Technol.* **21**, 1098 (2006).
- ²²N. Vukmirović, D. Indjin, Z. Ikonić, and P. Harrison, *Appl. Phys. Lett.* **88**, 251107 (2006).